Comparison of distinctive polymeric membrane structures as support materials for membrane extraction of chiral amines

Gilles Van Eygen[a,b,*], Stijn Keuppens[a], Xander De Breuck[a], Bianca Swankaert[c], Patrik Boura[a,d], Eva Loccufier[c], Juraj Kosek[d], Deepika Ramasamy[e], Fady Nahra[f,g], Anita Buekenhoudt[f], Karen De Clerck[c], Bart Van der Bruggen[a], Patricia Luis[b,h]

a Process Engineering for Sustainable Systems (ProcESS), Katholieke Universiteit Leuven, Celestijnenlaan 200f, 3001 Leuven (Belgium)

b Materials & Process Engineering (IMAP), Université catholique de Louvain, Place Sainte Barbe 2, B-1348 Louvain-la-Neuve (Belgium)

c Department of Materials, Textiles and Chemical Engineering (MaTCh), Technologiepark 70, 9052 Zwijnaarde (Belgium)

d Department of Chemical Engineering, University of Chemistry and Technology Prague, Technická 5, 166 28 Prague 6, Czech Republic

e Department 4MAT, Université Libre de Bruxelles, Avenue F.D. Roosevelt, 50 . CP 165/63, 1050 Bruxelles

f Unit Separation and Conversion Technology, Vlaamse Instelling voor Technologisch Onderzoek (VITO NV), Boeretang 200, 2400 Mol (Belgium)

g Department of Chemistry and Centre for Sustainable Chemistry, Ghent University, Krijgslaan 281 (S3), 9000 Ghent, Belgium

h Research & Innovation Centre for Process Engineering (ReCIPE), Place Sainte Barbe 2, bte L5.02.02, B-1348 Louvain-la-Neuve (Belgium), Tel: +32 (0)10 47 25 87 - Fax: +32(0)10 47 40 28

* Corresponding author: gilles.vaneygen@kuleuven.be

Keywords — polymers, supported liquid membranes, extraction technology

Abstract

This study investigates the synthesis and performance of polymeric membranes for their potential application in supported liquid membranes (SLM), using the extraction of α-methylbenzylamine (MBA), 1-methyl-3-phenylpropylamine (MPPA), and isopropyl amine (IPA) as a reference. Three synthesis methods — phase inversion, electrospinning, and stretching — were evaluated, each impacting the membrane morphology differently. The polymer selection influenced porosity, wettability, and surface free energy with PTFE exhibiting the highest hydrophobicity. Membrane wettability was assessed using the ionic liquid [P6,6,6,14][N(Tf)2] as the selective extractant, revealing that larger pore sizes enhanced the impregnation efficiency, while reducing the final SLM stability. Solute fluxes and selectivity were quantified; electrospun membranes exhibited higher fluxes, ranging from 1.0 to 1.2 g/(m²h) for MBA, 2.1 to 2.2 g/(m²h) for MPPA, and 0.8 to 1.2 g/(m²h) for IPA, along with a higher selectivity compared to phase inversion membranes, with fluxes ranging from 0.2 to 0.3 g/(m²h) for MBA, 0.2 g/(m²h) for MPPA, and 0.3 to 0.4 g/(m²h) for IPA. Stretched membranes demonstrated a comparable selectivity (MBA/IPA = 2.2, MPPA/IPA = 3.9), but reduced fluxes with increasing pore size, decreasing from 2.7 to 0.5 g/(m²h) for MBA, 4.9 to 0.9 g/(m²h) for MPPA, and 1.2 to 0.3 g/(m²h) for IPA, as the nominal pore size increased from 50 to 450 nm. This phenomenon likely resulted from the improved impregnation efficiency, coupled with a lower porosity and larger thickness in the membranes with larger pores. Overall, the membrane morphology significantly influenced the SLM performance and stability, with homogeneous, porous membranes possessing smaller pore sizes and high hydrophobicity exhibiting optimal characteristics. These findings underscore the critical role of membrane structure and properties in SLM applications.

Introduction

Chiral amines are widely used intermediates in active pharmaceutical ingredients (API), fine chemicals, and agrochemicals [1]. It is estimated that approximately 40 to 45 % of the drug candidates contain a chiral amine [2]. Chiral amines are mainly synthesised by traditional chemical methods using metals-based catalysts, which require harsh conditions or the use of expensive chiral ligands. Although research has already been performed on alternative synthesis strategies, such as photocatalysis [3], chemoenzymatic cascades [4], and improving existing enzymes [5], these methods have not yet reached their full industrial application. The use of biocatalytic synthesis reactions has been thoroughly researched with an increasing amount of enzymes in the toolbox in recent years [6]. However, chiral amine production is characterised by an unfavourable equilibrium reaction having only a 50 % yield [7], [8]. For this reason, *in situ* product removal (ISPR) can be used to improve both the product yield and the downstream processing [9].

Liquid-liquid extraction (LLE) is a widely employed ISPR technology in which a feed phase is mixed with an immiscible solvent phase. The solvent phase exhibits a higher affinity for the target solutes, enabling a selective separation. Typically, one phase is dispersed within the other, followed by solvent recovery through a subsequent separation stage, such as distillation, filtration, etc. [10], [11]. However, LLE encounters several inherent limitations, due to its time-consuming and laborious nature, along with the requirement for large quantities of toxic solvents, which are potentially harmful for human health and the environment. Additionally, emulsion formation can be problematic, while multiple LLE stages might be required for more complicated separations containing numerous target compounds with significant polarity differences [12]. Hence, it is essential to appropriately select the solvent to achieve a sustainable process while not posing challenges to large-scale industrial implementation. Apart from solvent selection, equipment design is another complication, as the main challenge in designing an LLE process is to maximise the mass transfer by creating as much interfacial area as possible between the feed and solvent phase. This is achieved by either using mixer-settlers or packed extraction columns. However, this conventional equipment has several drawbacks, including the need for dispersion and coalescence, emulsification problems, and flooding and loading limitations, apart from the requirement for a density difference between the phases and high maintenance costs for centrifugal apparatus [13], [14].

A possibility to overcome the inherent limitations of LLE is to combine membrane technology with LLE, which is referred to as membrane extraction (ME). Especially supported liquid membrane (SLM) extraction has shown promise as an alternative extraction technology. Within an SLM, the organic extractant is immobilised in the pores of a porous support material. Subsequently, the target solutes diffuse from the feed into the membrane phase, while simultaneously being stripped by the stripping phase [15], [16]. Using SLMs has different advantages over conventional LLE, as the extraction and stripping stage are combined into one unit, leading to lower operational costs compared to conventional separation technologies, such as distillation. Furthermore, only small amounts of the extractant are required [17], [18]. SLM systems have already been employed in both analytical and industrial fields for wastewater treatment, separation, and preconcentration, with a particular emphasis on metal recovery. Recently, research has focused on using SLMs for the separation of fine chemicals and drugs from wastewater. The capacity of SLMs to extract products in relatively small volumes positions them as an appealing alternative to crystallization, precipitation, distillation, and liquid-liquid extraction (LLE) for the pharmaceutical industry [19]. However, SLMs are used in very few

large-scale applications because of their poor membrane stability. This poor stability is mainly attributed to the loss of extractant from the pores, resulting in a tremendous decrease in solute flux and membrane selectivity. The membrane instability can be attributed to multiple causes, such as the presence of a transmembrane pressure, evaporation, and dissolution or dispersion into the adjacent phases [20], [21]. Additionally, the LM phase is kept in the pores through capillary forces making the bond relatively weak [7], [17], [22].

The SLM stability is affected by a variety of parameters, such as the support type and its pore radius, the solvent type of the liquid membrane, the interfacial tension between the aqueous and organic phase, the flow velocity of the aqueous phases, and the method of preparation [20]. Myriad strategies have already been used to overcome the stability issues of SLMs, either by changing the configuration of the setup, or by changing the solvent or support material. For example, opposed to using conventional organic solvents, either pure or diluted ionic liquids (ILs) can be used [23]. They are characterised by an extremely low volatility, next to a high chemical and thermal stability and a high viscosity, which might aid in preventing solvent loss due to evaporation or pressure gradients [24]–[27]. To further enhance the stability, other techniques could be used, such as the formation of barrier layers [28], and surface coating of the membranes [29].

Notably, the choice of the support material also affects the SLM stability and performance. In general, the support material of an SLM is selected based on its porosity, pore size, morphology, thickness, and its mechanical and chemical properties. A first key support property is the wettability of the membrane, which can be either hydrophilic or hydrophobic depending on its affinity for water molecules. Second, a high porosity is desirable, as the support porosity indicates the amount of LM phase that can be immobilised. Furthermore, a smaller pore size is favourable, due to the higher SLM stability. Third, the thickness of the support should be as thin as possible to reduce the membrane resistance without compromising the mechanical stability. Additionally, the tortuosity, which describes the deviation of the pores from a straight line, should be minimised to avoid a long diffusion path length. Last, the membrane should be chemically inert to avoid swelling or degradation when in contact with the adjacent phases. The most widely accepted support materials are polymers, such as poly(vinylidene fluoride) (PVDF), polypropylene (PP), polytetrafluoroethylene (PTFE), polycarbonate (PC), cellulose triacetate (CTA), and polyamide (PA), due to their low cost and facile synthesis procedures [21], [30].

Various fabrication techniques can be used, including sintering, stretching, track etching, interfacial polymerisation, phase inversion, and electrospinning, but the latter two are more commonly used in the membrane field. Generally, phase inversion membranes are synthesised by immersion precipitation, *i.e.*, a polymer solution is cast on a support material and then immersed in a coagulation bath containing a non-solvent. Solidification of the polymer then takes place, as the solvent is exchanged by the non-solvent. On the other hand, electrospinning fabricates fibres by employing an electrically charged jet of a polymer solution. Due to the presence of a potential gradient, the jet of the polymer solution erupts, and is consequently solidified after evaporation of the solvent [31]. It should be noted that for the synthesis of polymeric membranes generally toxic solvents are used, for example, N,N-dimethylformamide (DMF), N,N-dimethylacetamide (DMAc), and N-methylpyrrolidone (NMP), due to their strong dissolution power. Therefore, to allow for a truly green process, alternative solvents should be used for membrane fabrication [32].

The objective of this work is to study the effects of membrane morphology on the performance and stability of supported liquid membranes (SLM). To this end, various polymeric materials including polysulfone (PSf), poly(vinylidene fluoride) (PVDF), poly(vinylidene fluoride-co-hexafluoropropylene) (PVDF-co-HFP), polycaprolactone (PCL), polyamide 6 (PA-6), poly(ether-block-amide) (PEBA), and polytetrafluoroethylene (PTFE), were used for the fabrication of polymeric support materials using either phase inversion, electrospinning, or stretching. Various membrane properties, such as the porosity, wettability, and pore size, were analysed to study their effects on the final membrane performance focussing on one case study, namely the extraction of chiral amines. Specifically, an SLM was prepared using these supports and trihexyltetradecylphosphonium bis(trifluoromethylsulfonyl)-amide ([P6,6,6,14][N(Tf)2]) as the extractant. This choice follows from previous research demonstrating the selective and stable nature of this ionic liquid as an extractant [33]. The SLM should be selective towards the product amines α-methylbenzylamine (MBA) and 1-methyl-3-phenylpropylamine (MPPA) over the donor amine isopropyl amine (IPA). The performance of the SLMs considered was evaluated based on their stability, selectivity, and overall solute fluxes.

2. Materials and methods

2.1 Chemicals and membranes

The following chemicals were used for the membrane extraction experiments. Na_2CO_3 (≥ 99.5 %, Honeywell Fluka) and $NaHCO_3$ (≥ 99.7 %, Sigma-Aldrich) were used to prepare the feed buffer, while NaH_2PO_4 (≥ 99.0 %, Sigma-Aldrich) and H_3PO_4 (≥ 85 %, Sigma-Aldrich) were used to prepare the strip buffer. NaOH (≥ 98 %, Sigma-Aldrich) was used to prepare a solution for pH adjustment. The used amines were α-methylbenzylamine (MBA, 98 %, Sigma-Aldrich), 1-methyl-3-phenylpropylamine (MPPA, 98 %, Sigma-Aldrich), and isopropyl amine (IPA, ≥ 99.5 %, Sigma-Aldrich). Trihexyltetradecyl-phosphonium bis(trifluoromethylsulfonyl)amide ([P6,6,6,14][N(Tf)2], > 98 %, Iolitec) was used as the only extractant for the SLM experiments. Diiodomethane (> 99 %, Thermo Scientific) and glycerol (≥ 99 %, Fisher Chemical) were used for the surface free energy analysis. All chemicals were used without further purification.

Polysulfone (PSf, Mw ~ 22,000), poly(vinylidene fluoride) (PVDF, Mw ~ 275,000, Mn ~ 107,000), and poly(vinylidene fluoride-co-hexafluoropropylene) (PVDF-co-HFP) were purchased from Sigma-Aldrich for the preparation of the phase inversion membranes using N,N-dimethylformamide (≥ 99.9 %, Honeywell Riedel-de Haën™) as the solvent. For the preparation of the electrospun membranes, the poly(ether-block-amide) (PEBA-72, Pebax® Rnew®, 72R53 SP 01 resin) was kindly received from Arkema, while both polycaprolactone (PCL) and polyamide 6 (PA-6) were provided by Sigma-Aldrich. The solvents formic acid (FA, > 98 v%), acetic acid (AA, > 99.8 v%), and anisole (An, > 98 v%) were supplied by Sigma-Aldrich. All solvents were used as received. The stretched microfiltration ePTFE membranes (Tetratex®) with a nominal pore size of 50 nm (#1325), 200 nm (#1302), and 450 nm (#3103) were kindly provided by Donaldson. Moreover, a stretched PTFE membrane laminated on polypropylene (#6501, Donaldson) with a nominal pore size of 0.1 µm, was used as a support for the impregnation of the PTFE membranes.

2.2 Membrane synthesis, impregnation, and characterisation

2.2.1 Synthesis of phase inversion membranes

First, three polymer solutions were prepared as specified in Table 1. After addition of the polymer pellets, the solution was heated to 60 °C and stirred magnetically at 300 rpm for at least 24 hours. Afterwards, the solution was sonicated at 60 °C for 60 minutes to remove any remaining air bubbles.

Table 1. Process parameters for the synthesis of phase inversion membranes.

Nr.	*m*(PSf)	*m*(PVDF)	*m*(PVDF-co-HFP)	V(DMF)
	g	g	g	mL
1	4	0	0	20
2	0	4	0	20
3	0	0	4	20

The solutions were then cast on a glass plate using a Porometer Memcast™ casting machine at a temperature of 60 °C and using a casting knife thickness of 250 µm. The used casting speed was 0.2 cm/s. Once the casting knife passed the entire glass plate, it was removed and the membrane was left for one minute on the glass plate to evaporate the solvent. Then, the glass plate was put in a

coagulation bath with deionised water for 30 minutes. After coagulation, the membrane was removed from the bath and inserted into a vacuum oven at 60 °C and 60 mbar for one hour. To prevent the absorption of water from the air into the membrane, the membranes were stored in a desiccator.

2.2.2 Synthesis of electrospun membranes

All nanofibers were produced at a temperature of 23 ± 2 °C and a relative humidity of 50 ± 10 % with the aid of a high-voltage power supply (Glassman High Voltage Series). The process parameters for the electrospun membrane synthesis are given in Table 2. The spin conditions were determined by taking into account various factors including solvent selection for solubility and conductivity, solution viscosity, as well as temperature and humidity levels during the spinning process, as outlined in relevant literature [34]–[37].

Table 2. Process parameters for the synthesis of electrospun membranes. The used solvents were formic acid (FA), anisole (An), and acetic acid (AA).

Polymer	Concentration wt%	Solvent v%	Flow rate mL/h	Voltage kV	Tip-to-collector distance cm
PEBA-72	8	60/40 FA/An	2	30	6
PCL	23	70/30 FA/AA	1.5	22	10
PA-6	16	50/50 FA/AA	2	21-25	6

2.2.3 Membrane impregnation

To impregnate the support with the extractant, a vacuum pump was used to draw the extractant into the membrane. Circular membranes were cut with a diameter of 46 mm. A Whatman GF/C Glass microfiber filter paper (Ø = 90 mm, Cytiva) was used as a support for the phase inversion membranes, while a PTFE membrane laminated on polypropylene ((#6501, Donaldson) was used as a support for the stretched PTFE membranes. No filter paper was used for the electrospun membranes. Once the membrane was aspirated, a layer of the ionic liquid was pipetted on the membrane surface. An impregnation time of at least 45 minutes was used. The membranes were weighed before and after impregnation to determine the amount of absorbed extractant. The impregnation efficiency is defined as the amount of extractant absorbed divided by the membrane surface area:

$$\text{Impregnation efficiency (\%)} = \frac{m_{\text{wet}} - m_{\text{dry}}}{A} \cdot 100$$

in which m_{dry} (g) and m_{wet} (g) are the dry and wet membrane mass, respectively, and A (m²) the membrane surface area. Apart from the impregnation efficiency, the SLM stability is another important parameter, which can be quantified by the solvent residual as follows:

$$\text{Solvent residual (\%)} = \frac{m_{\text{after}} - m_{\text{dry}}}{m_{\text{wet}} - m_{\text{dry}}} \cdot 100$$

in which m_{after} (g) is the weight of the membrane after the experiment, and m_{dry} (g) and m_{wet} (g) are the weight of the membrane before and after impregnation.

2.2.4 Membrane characterisation

Contact angle measurements (CAM)

Contact angle measurements with Milli-Q water were performed for all the membrane materials using a Krüss DSA 10-Mk2 apparatus. This was done by cutting a square of approximately 1 cm^2 and forming a 4 µL droplet of Milli-Q water at a rate of 24.59 µL/min. The droplet was put onto the membrane using a syringe plunger. Thereafter, the contact angle was measured using the software Drop Shape Analysis. The measurement was performed every second for a period of 60 seconds. All measurements were performed in triplicate. A typical wetting profile of a porous support is given in Figure S1 in Section SD-1. For the surface free energy analysis, all measurements were conducted on the top side of the membranes. Each solvent was tested twice, and the mean value of the contact angle was used to calculate the surface free energy. The properties of the probe liquids, namely diiodomethane, water, and glycerol, are given in Table 3.

Table 3. Properties of the probe liquids for the surface free energy analysis [38].

Solvent	γ^{tot} mN/m	γ^{d} mN/m	γ^{p} mN/m
Diiodomethane	50.8	50.8	0
Water	72.8	21.8	51.0
Glycerol	64.0	34.0	30.0

Scanning electron microscopy (SEM)

To visualise the membrane structure and pore sizes, the membranes were analysed using an SEM ULTRA (Zeiss). Membrane samples of approximately 1 cm^2 were placed on an SEM holder and sputter coated with a gold layer of 1.5 to 2 nm (BALZERS UNION FL 9460 BALZERS SCD 030). A voltage of 5 kV was used to obtain an image of the membrane surface. To evaluate the cross section, the membranes were repeatedly dipped in deionised water and ethanol and consecutively immersed into liquid nitrogen. At these low temperatures, the membranes became brittle and could be broken without deforming the cross section [39].

Determination of gas permeability, pore diameter, and pore distribution

The gas permeability and pore size of the electrospun and stretched membranes was determined using the gas-liquid porometer Porolux™ 1000. The porous membrane samples (⌀ = 2.5 cm) were first immersed in FC-40 wetting liquid overnight. Then, a flow of pressurised gas was applied to the porous membrane sample and the gas flow through the sample was measured, as the liquid was displaced out of the porous membrane. Larger pores become empty first and so do the smaller pores, as the applied pressure increases, until all through pores are empty. This measurement resulted in the “wet” curve, which represents the measured gas flow in function of the applied pressure. The “wet” curve was then compared to the “dry” curve, which plots the gas flow in function of the applied pressure for the dry sample. Based on the “wet”, “dry” and “half-dry” curve (which represents the flow values of the dry curve divided by two), information can be obtained about the pore structure. Four samples were analysed from each membrane.

To further characterise the membrane morphology quantitatively, a Quantachrome PoreMaster 33 was employed to analyse the samples by low and high pressure mercury intrusion porosimetry (MIP) reaching pressures up to 414 MPa. This allows the determination of pore sizes in the range from 1 mm down to 3 nm. Samples were cooled in liquid nitrogen and cut by a scalpel prior to the measurement, while high pressure MIP was measured in Autospeed mode. Pore number fraction (PNF), *i.e.,* the number of pores in a narrow range of pore sizes relative to the total number of pores in the measurement range, was evaluated using the Quantachrome Instruments Poremaster software, under the assumption of cylindrical pores. The average pore size was then calculated as:

$$Dp_{average} = \sum_{n=1}^{\infty} (PNF(i) \bullet Dp(i))$$

where $Dp(i)$ represents a narrow pore size range, specific to $PNF(i)$. Additionally, the sample porosity was determined based on gravimetric analysis of MIP. The mercury porosimetry results should be interpreted with caution as the sample compression can affect the results.

2.4 Membrane extraction experiments

For the extraction experiments, a feed (pH 10) and strip buffer (pH 3) were prepared. More specifically, 7.58 g of Na_2CO_3 and 10.76 g of $NaHCO_3$ were added to 1 L of Milli-Q water under continuous stirring. After full dissolution, 500 mg of MBA, MPPA, and IPA were added to the feed solution. The strip buffer was prepared by adding 21.98 g of NaH_2PO_4 and 1724 µL of a 85 % (w/w) H_3PO_4 solution to 1 L of Milli-Q water. After full dissolution, the pH was measured for both solutions.

The experimental setup used for the membrane extraction experiments is given schematically in Figure 1. The experiments ran for 24 hours in a counter-current setup, driven by two magnetically driven gear pumps. A frequency drive (Flowtec) was used to control the flow rate. Flow rates were set at 10 L/h and monitored using two variable-area flow meters with a valve (100-1000 mL/min, Masterflex). The pressure was monitored through the use of four diaphragm gauge guards with a manometer (Series 3D, 0-6 bar, EM-Technik). For every experiment, a volume of 250 mL was used for both the feed and the strip buffer. The temperature of the buffer solutions was kept constant at 30 °C $\pm$ 2 by means of a circulating thermostatic bath (Kiss K6, Huber). The temperature was monitored regularly through an RTD thermometer (DIGI-SENSE). The membranes were clamped in a Teflon membrane cell with a spiral pattern to maximise the contact area between the buffers and the membrane. Additionally, the membranes were weighed before and after each experiment to determine the amount of extractant loss.

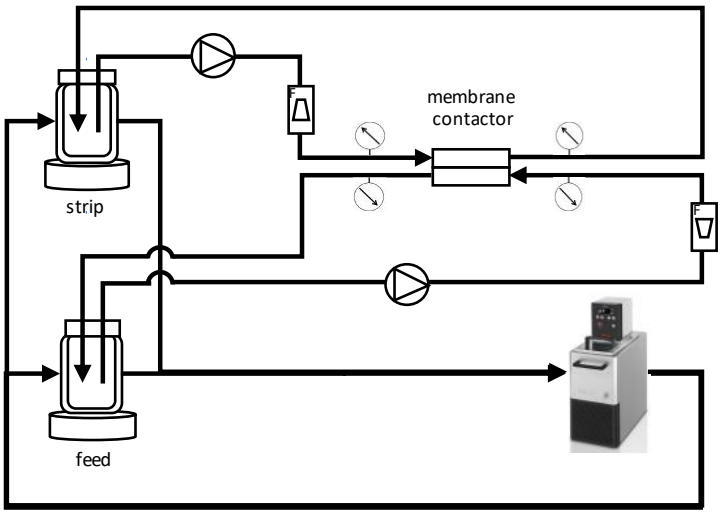

Figure 1. Schematic diagram of the used membrane extraction setup.

Samples of both the feed and strip buffer were taken at fixed intervals, namely at the start of the experiment and after 1, 3, 6, and 24 hours. At each time point, 1 mL of the feed and strip solution was pipetted and added to an HPLC and GC vial. To the GC samples, 200 µL of a 25 % NaOH solution was added. For the analysis of MBA and MPPA, an HPLC-UVVIS system (Schimadzu Prominence-I LC-2030C 3D) was used with acetonitrile and an 0.1 v% H_3PO_4 solution as the mobile phases. For the analysis of IPA, a headspace GC-FID Autosystem XL (PerkinElmer) with an Rtx-5 Amine column (30 m, 0.25 mm, 0.50 µm) was used with helium as the mobile phase.

2.5 COSMO-RS simulations

First, quantum calculations employing density functional theory (DFT) with a resolution identity (RI) approximation were conducted using the TmoleX v. 4.5 software package. The optimised geometries of the polymers under consideration (refer to Section SD-2 for their structures) were obtained using a triple zeta valence polarised basis set (def-TZVP) at the Becke-Perdew (BP-86) functional level of theory, and incorporating the COSMO solvation model. These optimised geometries were stored as COSMO files. Second, vibrational frequency calculations were carried out to validate the presence of an optimised energy state. Third, the generated COSMO files were used as input in COSMOthermX to analyse the σ-profiles and -surfaces of the polymers under investigation. The polymeric materials were approximated using a short oligomeric chain of maximum four monomeric units [40]–[42].

3 Results and discussion

3.1 Membrane characterisation

Both the synthesis method and the polymer choice strongly influence the membrane properties. Seven base polymer materials were used with various molecular structures to test the effect of the polymer on the membrane properties. More specifically, polysulfone (PSf), polyvinylidene fluoride (PVDF), and poly(vinylidene fluoride-co-hexafluoropropylene) (PVDF-co-HFP) were used for the synthesis of phase inversion membranes, while a polyether-block-amide (PEBA-72), polycaprolactone (PCL), and a polyamide (PA-6) were used for the synthesis of electrospun membranes. The stretched polytetrafluoroethylene (PTFE) membranes were obtained commercially.

3.1.1 COSMO-RS simulations

The molecular structures of the considered polymeric materials are given in Figure S2 in Section SD-2 together with their σ-surfaces. Their affinity for other compounds can be analysed by the σ-profile (see Figure S3), as this profile provides a distribution histogram of the charge density σ over the molecular surface. For σ < -0.0085 e/Å² and σ > 0.0085 e/Å², the molecular surface may act as either a hydrogen bond donor or acceptor, respectively, while the surface has a nonpolar character if σ is in the range [-0.0085, 0.0085] e/Å² [43]. As can be seen in Figure S3, both PVDF-co-HFP and PTFE have their highest peaks in the nonpolar region, making them the most hydrophobic. Although PVDF has a very similar structure as PVDF-co-HFP, its peaks in the nonpolar region are much less pronounced. The repetitive carbon side chain with three fluorine atoms in PVDF-co-HFP most likely imparts a more nonpolar character. Both PA-6 and PCL have their main peaks in the nonpolar region, but also have a small peak in the hydrogen bond acceptor region. Similar observations can be made for PSf. However, PEBA has peaks in both the hydrogen bond donor and acceptor region. This can also be seen in the σ-surface of PEBA, which shows various electrostatically dense regions across its molecular surface.

3.1.2 Morphology, wettability, and surface free energy

The membrane morphology is strongly influenced by the synthesis method, for example, both the pore size and porosity can vary significantly between fabrication techniques. As can be seen in Figure S4 in Section SD-3, phase inversion membranes show an asymmetric structure with a dense top layer and a porous bottom layer, which was also reported by Galiano [44]. As the top side is in direct contact with the aqueous non-solvent phase, this ensures a rapid phase inversion (*i.e.*, solvent evaporation) and, hence, a dense layer due to the higher polymer concentration (see Figure S4 (a)-(c)). The bottom side, on the other hand, is in contact with the glass plate, which leads to a slow phase separation and thus a more porous structure [45]. This asymmetric structure is especially visible for the PVDF membrane, whilst the PSf and PVDF-co-HFP membrane provide a denser membrane. On the other hand, more open and porous structures can be obtained using electrospinning and stretching (see Figure S5 in Section SD-3). The porosity of both the electrospun and stretched membranes has been quantified further and is given in Figure 6 (b) and Figure 7 (b). As can be seen in Figure S5 (a), the stretched PTFE film shows an expanded structure, which occurs because the membrane stretching process involves extruding a polymer powder and consecutively stretching it in the extrusion direction, resulting in partial film expansion [31]. Opposed to the stretched film, the electrospun membranes

have a symmetric network structure consisting of long fibres as well as a very high porosity (see Figure S5 (b)-(d)).

In addition to the morphology of the membrane, the membrane wettability or wetting behaviour is another important property affecting the SLM performance. According to Figure 2 (a), all phase inversion membranes show low contact angles (< 90°) indicating a more hydrophilic nature. On the other hand, both the electrospun and stretched membranes show contact angles above 120° (see Figure 3 (a) and Figure 4 (a)). Despite PTFE and PVDF-co-HFP having similar molecular structures and σ-profiles, their membranes show a distinct wetting behaviour, with the PVDF-co-HFP membrane showing a contact angle of 76.6° compared to 124.9° for the PTFE membrane.

An additional parameter is the membrane surface free energy, which is defined as the excess energy needed to increase the surface area of a solid [46]. In general, a higher surface free energy is associated with a higher degree of wettability, hence a more hydrophilic surface [47]. The surface free energy was determined using two different methods, which are based on contact angle measurements of three probe liquids. The value of the contact angle is a function of both the membrane surface free energy and the liquid properties. The two considered methods are OWRK/Fowkes, and Wu (see Section SD-4) [48]. The Wu and OWRK methods give similar results, as they both rely on the principle of splitting the surface free energy into a dispersive and polar component. They only differ in the way the mean is calculated, *i.e.*, Wu found that the geometric mean underestimated the polar interaction, hence they employed a harmonic mean [47]. Based on Figure 4 (b), PTFE has a very low surface free energy and therefore the least favourable wettability, while PCL has the highest surface free energy (see Figure 3 (b)). All the phase inversion membranes show an intermediate wettability behaviour (see Figure 2 (b)). These results can be linked to the contact angles of the probe liquids, as all phase inversion membranes show similar contact angles, while PTFE shows the highest contact angles of all membranes. PCL, on the other hand, shows a contact angle of zero for diiodomethane, which explains its high surface free energy. The mean values of the contact angle measurements are given in Table S1 in Section SD-4.

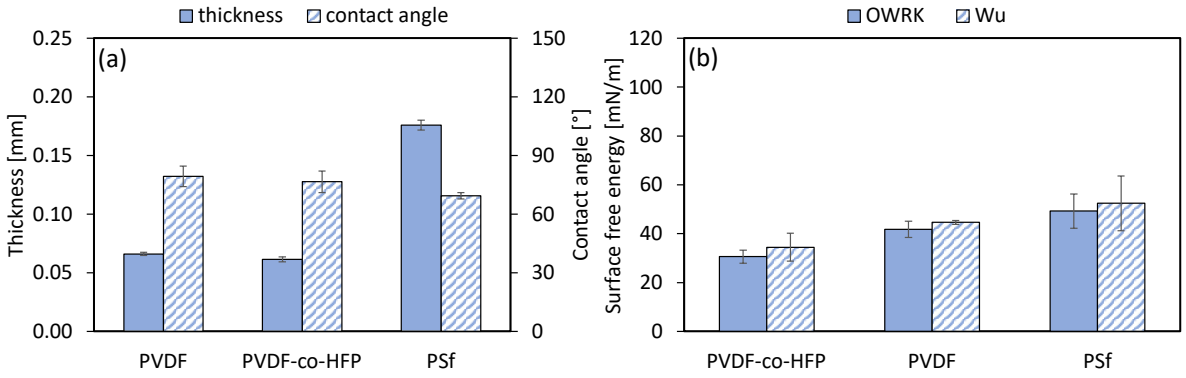

Figure 2. Experimental results of (a) the thickness and contact angle, and (b) the surface free energy of the phase inversion membranes.

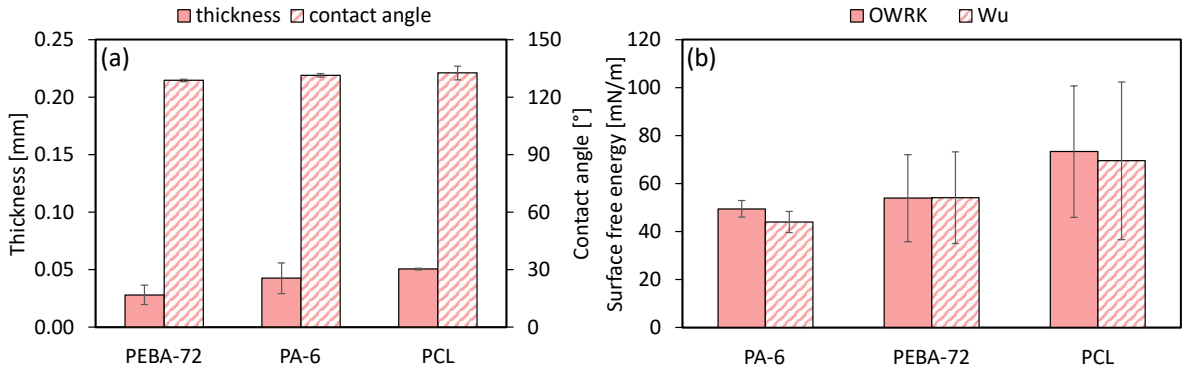

Figure 3. Experimental results of (a) the thickness and contact angle, and (b) the surface free energy of the electrospun membranes.

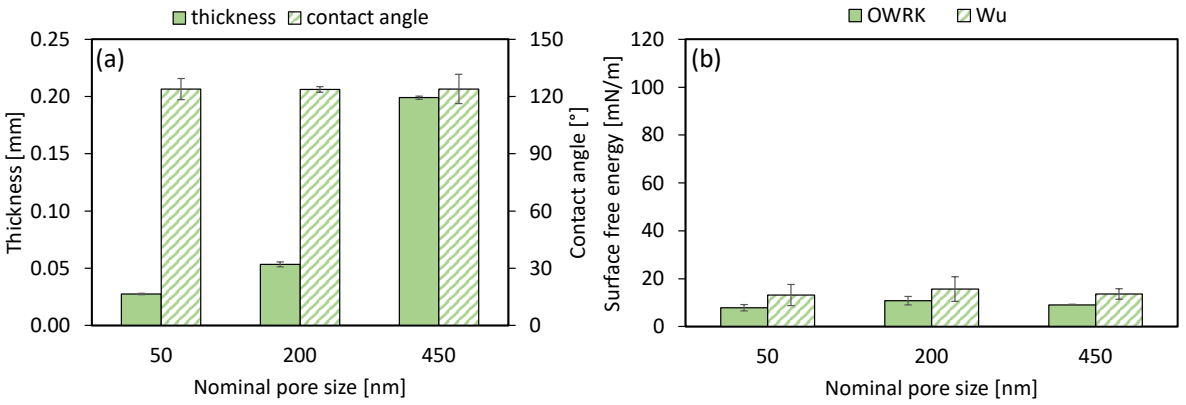

Figure 4. Experimental results of (a) the thickness and contact angle, and (b) the surface free energy of the stretched PTFE membranes.

3.2 Membrane extraction performance

3.2.1 Wetting efficiency and SLM stability

An important factor in SLM design is the wettability of the support material for the extractant, which can be quantified using the impregnation efficiency as defined in Section 2.2.3. For the phase inversion membranes, PVDF-co-HFP has the lowest impregnation efficiency (see Figure 5 (a)), which can be linked to its low surface free energy (see Figure 2 (b)). Similarly, PSf has the largest impregnation efficiency and the highest surface free energy, while PVDF has intermediate values. Additionally, PSf is more hydrophilic than PVDF and PVDF-co-HFP according to COSMO-RS, which could be beneficial for its impregnation. All phase inversion membranes have a desirable solvent residual above 90 % as can be seen in Figure 5 (b), which is most likely due to their denser structure.

The impregnation efficiency of the electrospun membranes exhibits an inverse relationship with the residual solvent content, as depicted in Figure 6 (a)-(b). This correlation is logical, given that a higher impregnation efficiency suggests easier solvent penetration into the membrane, thereby also implying that the solvent might escape more easily from the membrane. This phenomenon correlates with membrane porosity: a higher porosity corresponds to a lower impregnation efficiency, as more volume needs to be wetted. For materials with a lower porosity, on the other hand, after impregnation of the internal porous structure, additional extractant can be added as a layer on the surface, which could be washed away more easily, resulting in lower solvent residuals. The PA-6 membrane with a lower porosity (51.4 %) exhibits a higher impregnation efficiency and lower solvent residual compared to the more porous PEBA-72 membrane (80.6 %). Notably, the PCL membrane, despite having a higher porosity (66.0 %) than PA-6, demonstrates a higher impregnation efficiency and lower solvent residual. This could be attributed to the much larger nominal pore size of the PCL membrane. More specifically, a larger pore size would facilitate solvent penetration inside the porous membrane structure improving the impregnation dynamics. Conversely, a larger pore size may allow solvent droplets to escape and emulsify more easily, potentially leading to reduced solvent residuals. Notably, a large variation in the porosity was found for the electrospun membranes, ranging from 50 % for PA-6 to 80 % for PEBA-72. While Das and Gebru [31] mentioned that electrospinning generally leads to highly porous membranes having a porosity of over 80 %, lower porosities can thus also be obtained.

Similar trends can be observed for the stretched membranes (see Figure 7 (a)), *i.e.*, a higher pore size and lower porosity leads to improved impregnation efficiency and a lower solvent residual. For the stretched PTFE membranes, an inverse trend in the porosity can be seen for an increasing nominal pore size (see Figure 7 (b)). During the stretching, a polymer powder is extruded and stretched in the extrusion direction, which leads to expansion of the polymer film, as described by Das and Gebru [31]. However, depending on the stretching parameters, such as the longitudinal and transverse stretching rate and ratio, a variation in the porosity and pore size could be obtained. More specifically, Hao et al. [49] found that for an increase in the transverse stretching rate, the porosity becomes higher and the average pore size declines, which could explain the inverse trend in Figure 7 (b).

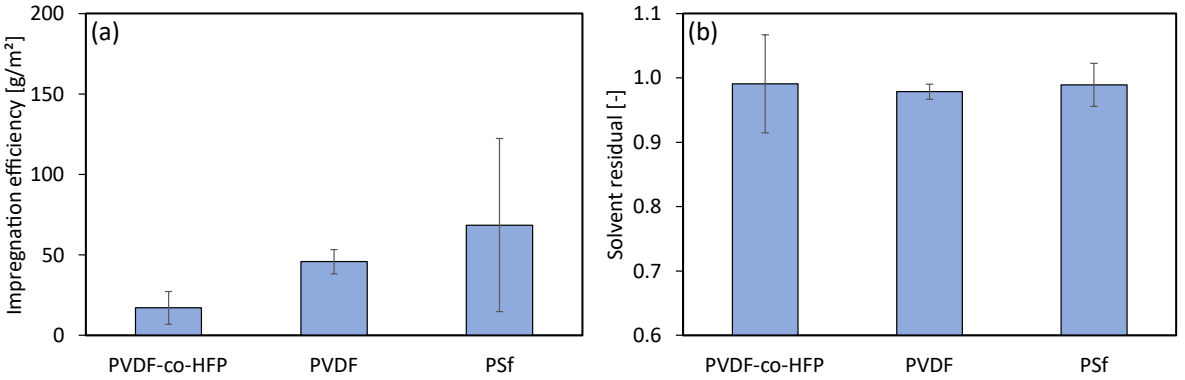

Figure 5. Experimental results of (a) the impregnation efficiency and solvent residual, and (b) the maximum and average pore size of the phase inversion membranes.

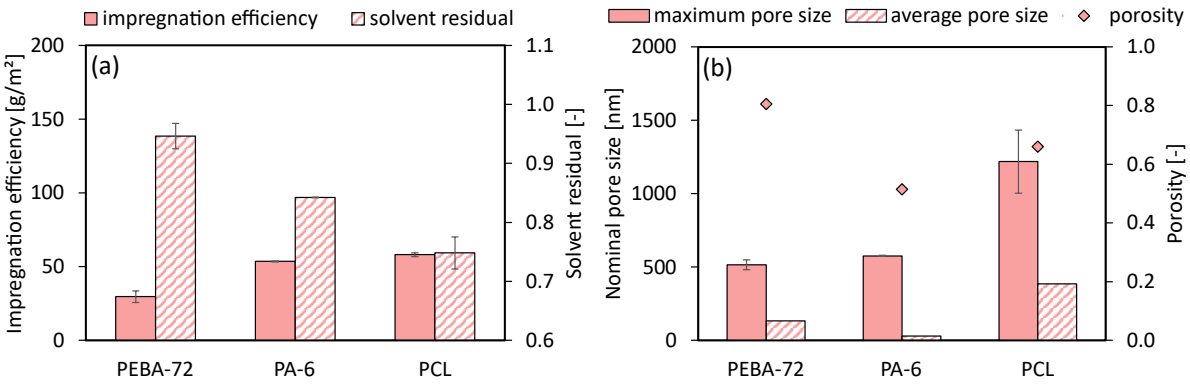

Figure 6. Experimental results of (a) the impregnation efficiency and solvent residual, and (b) the maximum and average pore size of the electrospun membranes.

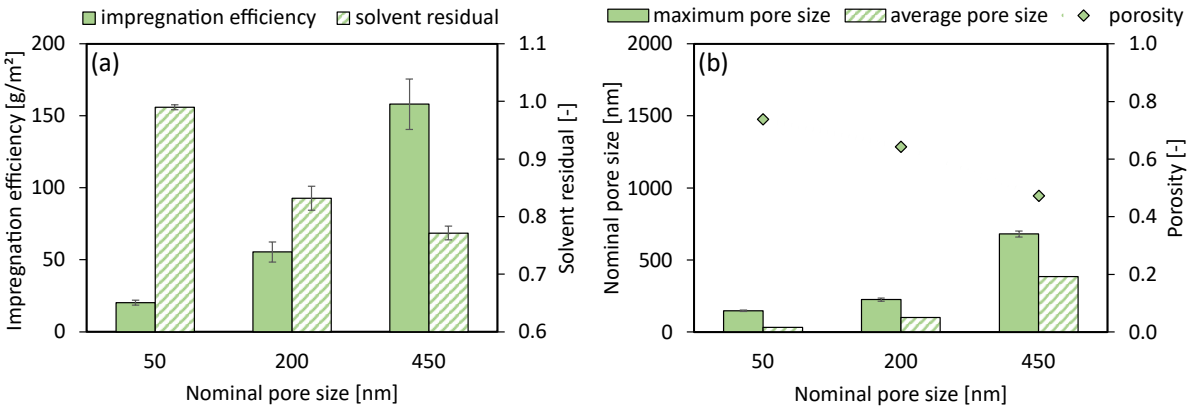

Figure 7. Experimental results of (a) the impregnation efficiency and solvent residual, and (b) the maximum and average pore size of the stretched membranes.

3.2.2 SLM extraction performance

The membrane extraction performance can be quantified by the transmembrane flux of the considered solutes MBA, MPPA, and IPA, and their selectivity. The flux and selectivity definition and their calculation procedure are given in Section SD-5. For the phase inversion membranes, the obtained fluxes are given in Figure 8 (a). Both the PSf and PVDF membrane show very low MBA and MPPA fluxes even lower than 0.5 g/(m²h), while their IPA flux is significantly higher. On the other hand, the PVDF-co-HFP membrane showed a decreased IPA flux leading to a higher affinity for both MBA and MPPA. Nonetheless, the selectivity of the phase inversion membranes is not suitable for the considered application. The drop in the solute fluxes is most likely due to the inherent morphology of the phase inversion membranes, *i.e.*, an asymmetric structure with a dense top layer. The solute transport would then be strongly influenced by the affinity with the membrane phase. More specifically, as the phase inversion membranes show a much lower water contact angle between 70 and 80° (see Figure 2 (a)), they all show a higher affinity towards the hydrophilic IPA molecule.

On the other hand, electrospun membranes exhibit improved performance in both fluxes and selectivity, as illustrated in Figure 9 (a) and (b). Their fluxes notably surpass those of phase inversion membranes, indicating that a porous network structure can positively affect fluxes, likely by enhancing solute diffusion. Although all electrospun membranes demonstrate similar fluxes, there is a slight decreasing trend in the following order: PEBA-72 > PA-6 > PCL, possibly correlated with an increasing membrane thickness in the same order. The selectivity remains consistent across all electrospun membranes, as all the membranes have a similar hydrophobicity based on their contact angle data (see Table S1 in Section SD-4).

An even better result can be obtained with the stretched PTFE membranes. More specifically, for the PTFE membrane with a pore size of 50 nm, the MBA and MPPA flux doubled compared with the electrospun membranes (see Figure 10 (a)). The selectivity remains semi-constant with a variation in the pore size (see Figure 10 (b)), while the fluxes drop significantly when the nominal pore size increases from 50 to 450 nm. This result might seem counter-intuitive, but the larger pore size also improves the impregnation efficiency (see Figure 7 (a)). Thus, more of the viscous extractant is present inside the membrane which slows down the solute diffusion. Additionally, the small-pore PTFE membrane has a lower thickness (see Figure 4 (a)) and higher porosity (see Figure 7 (b)). Hence, it can be stated that the diffusion flux through the membrane is directly proportional to its thickness and porosity. Table 4 provides a comparison of the flux results from this study with existing literature data on SLM extraction of amine compounds. It is important to note that the fluxes vary significantly due to different conditions used in other studies, such as feed concentration and extractant phase. Despite these variations, the results from the current study are notably higher than those reported in the literature. In conclusion, it could be stated that the stretched PTFE membrane with the lowest pore size provided the best performance in terms of stability and fluxes, while giving a satisfactory selectivity.

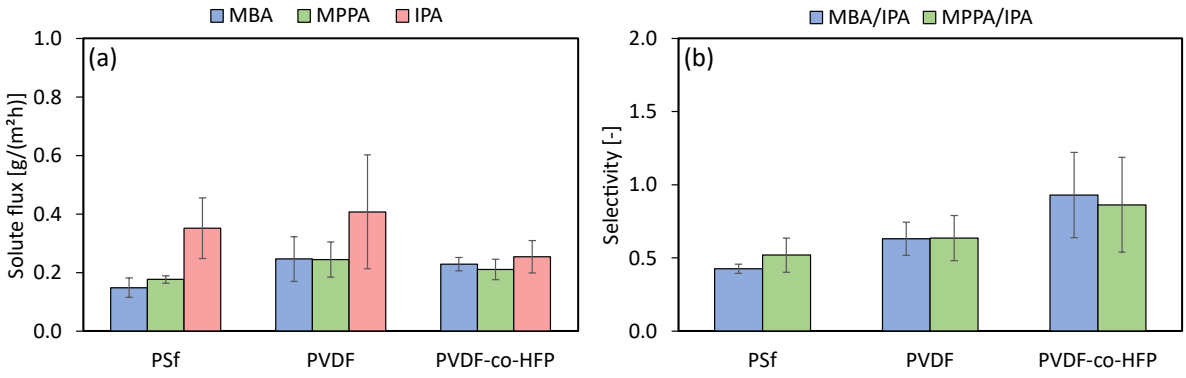

Figure 8. Experimental results of (a) the averaged solute fluxes from the feed phase, and (b) the MBA/IPA and MPPA/IPA selectivity for supported liquid membrane extraction using the phase inversion membranes.

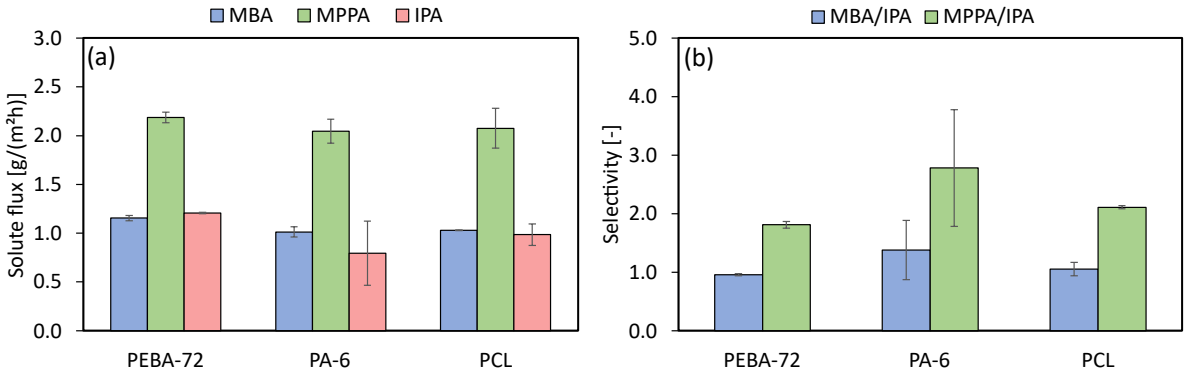

Figure 9. Experimental results of (a) the averaged solute fluxes from the feed phase, and (b) the MBA/IPA and MPPA/IPA selectivity for supported liquid membrane extraction using the electrospun membranes.

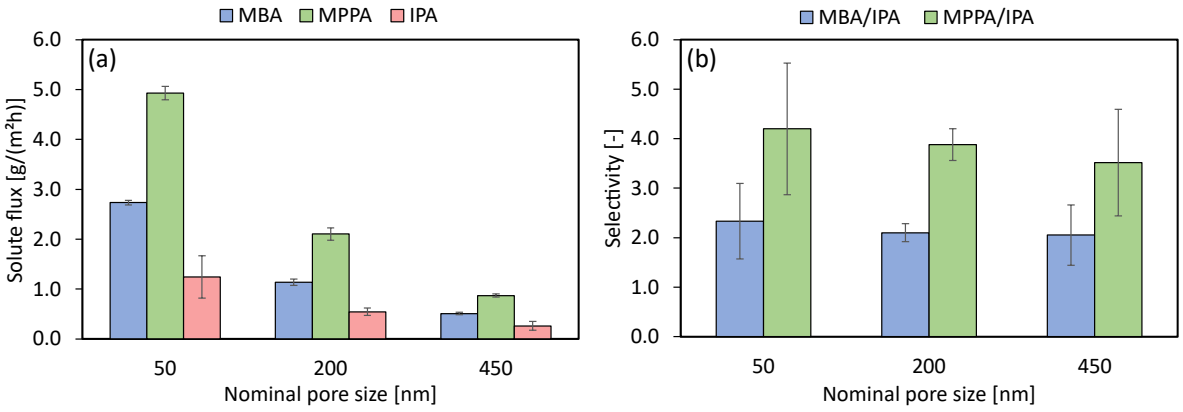

Figure 10. Experimental results of (a) the averaged solute fluxes from the feed phase, and (b) the MBA/IPA and MPPA/IPA selectivity for supported liquid membrane extraction using the stretched PTFE membranes.

Table 4. Comparison of the obtained fluxes with literature data.

	MBA		MPPA		IPA	
Ref.	*C*	*J*	*C*	*J*	*C*	*J*
-	g/L	g/(m²h)	g/L	g/(m²h)	g/L	g/(m²h)
[8]	0.12	0.06	-	-	-	-
[50]	2.42	0.67	2.98	0.64	59.11	0.08
This study	0.50	2.73	0.50	4.93	0.50	1.24

4 Conclusion

In this study, various polymeric membranes were explored for their suitability as support materials in supported liquid membrane (SLM) extraction of *α*-methylbenzylamine (MBA), 1-methyl-3-phenylpropylamine (MPPA), and isopropyl amine (IPA). The impact of membrane production methods and polymer choices on membrane characteristics such as hydrophobicity, porosity, pore size, and wettability was investigated. Three synthesis methods — phase inversion, electrospinning, and stretching — yielded membranes with distinct morphologies. Phase inversion produced asymmetric membranes with a dense top layer, while electrospinning and stretching resulted in homogeneous, interconnected membranes with a porous network structure.

Polymer selection influenced porosity, wettability, and surface free energy, with COSMO-RS simulations revealing PTFE and PVDF-co-HFP as the most hydrophobic polymers. Furthermore, larger pore sizes facilitated extractant penetration into the membrane pores, enhancing impregnation efficiency, and consequently, also the removal of the LM phase from the pores, when brought in contact with flowing phases. Solute fluxes and selectivity for MBA and MPPA over IPA determined the overall SLM performance. Phase inversion membranes exhibited low solute fluxes and lacked selectivity, attributed to their denser structure and hydrophilicity. Electrospun membranes showed increased fluxes and selectivity due to their porous structure, while stretched membranes maintained selectivity despite flux reduction at larger pore sizes.

In conclusion, membrane morphology significantly influenced SLM performance and LM stability. Phase inversion membranes offered high stability, but were unsuitable as an SLM support due to their denser structure and higher hydrophilicity. On the other hand, both the stretched and electrospun membranes improved fluxes and selectivity due to their porous and homogeneous network structure. A larger pore size leads to a reduced SLM stability, while a less porous membrane with a larger thickness led to lower solute fluxes. Notably, the stretched PTFE membrane with a 50 nm nominal pore size exhibited optimal performance in terms of fluxes, selectivity, and stability for the extraction process.

Acknowledgement

The authors extend their sincere gratitude to the following individuals whose contributions were instrumental in the completion of this research: Stijn Keuppens and Xander De Breuck, for their dedicated efforts in conducting the experimental work. Bianca Swankaert and Eva Loccufier, for the synthesis of the electrospun membranes and their valuable revisions to the manuscript. Special thanks

to Karen De Clerck for her supervision and guidance. Patrik Boura and Juraj Kosek, for their meticulous measurements and analyses using mercury porosimetry. Deepika Ramasamy and Fady Nahra, for their expertise in conducting gas permeability and porosity testing, which significantly enhanced the quality of the research. Anita Buekenhoudt, for her insightful discussions on the results, which greatly enriched our understanding. João A. P. Coutinho, for his valuable contributions to the discussion of COSMO-RS results, which added depth to our analysis. We also acknowledge the invaluable support and guidance provided by our supervisors, Bart Van der Bruggen and Patricia Luis, who played pivotal roles in the discussions of results and manuscript revision. Financial support for this research was generously provided by the Flemish Strategic Basic Research Program of the Catalisti cluster and Flanders Innovation & Entrepreneurship through the EASiCHEM project (contracts HBC.2018.0484 and K200522N).

Conflict of interest statement

The authors declare that there is no conflict of interest.

Declaration of generative AI and AI-assisted technologies in the writing process

During the preparation of this work the authors used ChatGPT, developed by OpenAI, in order to assist in drafting and refining this manuscript. After using this tool/service, the authors reviewed and edited the content as needed and take full responsibility for the content of the publication.

References

[1] F. Mutti, “Molecular science: The importance of sustainable manufacturing of chiral amines,” 2020. https://www.openaccessgovernment.org/chiral-amines/52451/.

[2] D. Ghislieri *et al.*, “Engineering an enantioselective amine oxidase for the synthesis of pharmaceutical building blocks and alkaloid natural products,” *J. Am. Chem. Soc.*, vol. 135, no. 29, pp. 10863–10869, 2013, doi: 10.1021/ja4051235.

[3] M. Leone, J. P. Milton, D. Gryko, L. Neuville, and G. Masson, “TBADT-Mediated Photocatalytic Stereoselective Radical Alkylation of Chiral N-Sulfinyl Imines: Towards Efficient Synthesis of Diverse Chiral Amines,” *Chem. - A Eur. J.*, vol. 30, p. e202400363, 2024, doi: 10.1002/chem.202400363.

[4] F. Chang, C. Wang, Q. Chen, Y. Zhang, and G. Liu, “A Chemoenzymatic Cascade Combining a Hydration Catalyst with an Amine Dehydrogenase: Synthesis of Chiral Amines,” *Angew. Chemie - Int. Ed.*, vol. 61, p. e202114809, 2022, doi: 10.1002/anie.202114809.

[5] Y. Fukawa, K. Yoshida, S. Degura, K. Mitsukura, and T. Yoshida, “Improvement of (S)-selective imine reductase GF3546 for the synthesis of chiral cyclic amines,” *Chem. Commun.*, vol. 58, pp. 13222–13225, 2022, doi: 10.1039/d2cc05116h.

[6] J. Østerby and J. M. Woodley, “Considerations for the Scale-up of in vitro Transaminase-Catalyzed Asymmetric Synthesis of Chiral Amines,” *ChemCatChem*, vol. 15, p. e202300560, 2023, doi: 10.1002/cctc.202300560.

[7] G. Rehn, P. Adlercreutz, and C. Grey, “Supported liquid membrane as a novel tool for driving the equilibrium of ω-transaminase catalyzed asymmetric synthesis,” *J. Biotechnol.*, vol. 179, no. 1, pp. 50–55, 2014, doi: 10.1016/j.jbiotec.2014.03.022.

[8] G. Rehn, B. Ayres, P. Adlercreutz, and C. Grey, “An improved process for biocatalytic asymmetric amine synthesis by in situ product removal using a supported liquid membrane,” *J. Mol. Catal. B Enzym.*, vol. 123, pp. 1–7, 2016, doi: 10.1016/j.molcatb.2015.10.010.

[9] P. Tufvesson, J. Lima-Ramos, J. S. Jensen, N. Al-Haque, W. Neto, and J. M. Woodley, “Process considerations for the asymmetric synthesis of chiral amines using transaminases,” *Biotechnol. Bioeng.*, vol. 108, no. 7, pp. 1479–1493, 2011, doi: 10.1002/bit.23154.

[10] D. B. Todd, “Solvent Extraction,” in *Fermentation and Biochemical Engineering Handbook: Principles, Process Design, and Equipment: Third Edition*, 2014.

[11] Z. Berk, *Food Process Engineering and Technology: Third Edition*. London : Academic P., 2018.

[12] R. Urkude, V. Dhurvey, and S. Kochhar, “15 - Pesticide Residues in Beverages,” in *Quality Control in the Beverage Industry*, 2019, pp. 529–560.

[13] H. Hashemi-Moghaddam, “Liquid-liquid extraction in the food industry,” in *Extraction Processes in the Food Industry*, 2024.

[14] A. Baudot, J. Floury, and H. E. Smorenburg, “Liquid-liquid extraction of aroma compounds with hollow fiber contactor,” *AIChE J.*, vol. 47, no. 8, pp. 1780–1793, 2001, doi: 10.1002/aic.690470810.

[15] P. Luis, *Fundamental Modelling of Membrane Systems*. Elsevier, 2018.

[16] G. Gong, H. Nagasawa, M. Kanezashi, and T. Tsuru, “Reverse osmosis performance of layered-hybrid membranes consisting of an organosilica separation layer on polymer supports,” *J. Memb. Sci.*, vol. 494, pp. 104–112, 2015, doi: 10.1016/j.memsci.2015.07.039.

[17] P. Dzygieł and P. P. Wieczorek, *Supported Liquid Membranes and Their Modifications: Definition, Classification, Theory, Stability, Application and Perspectives. Definition, Classification, Theory, Stability, Application and Perspectives.* 2009.

[18] M. Baczyńska, M. Waszak, M. Nowicki, D. Przadka, S. Borysiak, and M. Regel-Rosocka, “Characterization of Polymer Inclusion Membranes (PIMs) Containing Phosphonium Ionic Liquids as Zn(II) Carriers,” *Ind. Eng. Chem. Res.*, vol. 57, no. 14, pp. 5070–5082, 2018, doi: 10.1021/acs.iecr.7b04685.

[19] M. Farah, J. Giralt, F. Stüber, J. Font, A. Fabregat, and A. Fortuny, “Supported liquid membranes for the removal of pharmaceuticals from aqueous solutions,” *J. Water Process Eng.*, vol. 49, no. September, p. 103170, 2022, doi: 10.1016/j.jwpe.2022.103170.

[20] M. A. Malik, M. A. Hashim, and F. Nabi, “Ionic liquids in supported liquid membrane technology,” *Chem. Eng. J.*, vol. 171, no. 1, pp. 242–254, 2011, doi: 10.1016/j.cej.2011.03.041.

[21] L. J. Lozano, C. Godínez, A. P. de los Ríos, F. J. Hernández-Fernández, S. Sánchez-Segado, and F. J. Alguacil, “Recent advances in supported ionic liquid membrane technology,” *J. Memb. Sci.*,

vol. 376, no. 1, pp. 1–14, 2011, doi: 10.1016/j.memsci.2011.03.036.

[22] Z. Wang *et al.*, “Simultaneous extraction and recovery of gold(I) from alkaline solutions using an environmentally benign polymer inclusion membrane with ionic liquid as the carrier,” *Sep. Purif. Technol.*, vol. 222, no. 2, pp. 136–144, 2019, doi: 10.1016/j.seppur.2019.04.030.

[23] G. Van Eygen, B. Van der Bruggen, A. Buekenhoudt, and P. Luis Alconero, “Efficient membrane-based affinity separations for chemical applications: A review,” *Chem. Eng. Process. - Process Intensif.*, vol. 169, p. 108613, Dec. 2021, doi: 10.1016/j.cep.2021.108613.

[24] I. Cichowska-Kopczyńska, M. Joskowska, B. Debski, R. Aranowski, and J. Hupka, “Separation of toluene from gas phase using supported imidazolium ionic liquid membrane,” *J. Memb. Sci.*, vol. 566, no. May, pp. 367–373, 2018, doi: 10.1016/j.memsci.2018.08.058.

[25] A. Dahi *et al.*, “Supported ionic liquid membranes for water and volatile organic compounds separation: Sorption and permeation properties,” *J. Memb. Sci.*, vol. 458, pp. 164–178, 2014, doi: 10.1016/j.memsci.2014.01.031.

[26] A. P. de los Ríos, F. J. Hernández-Fernández, F. Tomás-Alonso, J. M. Palacios, and G. Víllora, “Stability studies of supported liquid membranes based on ionic liquids: Effect of surrounding phase nature,” *Desalination*, vol. 245, no. 1–3, pp. 776–782, 2009, doi: 10.1016/j.desal.2009.02.051.

[27] Y. Jiang, Y. Wu, W. Wang, L. Li, Z. Zhou, and Z. Zhang, “Permeability and Selectivity of Sulfur Dioxide and Carbon Dioxide in Supported Ionic Liquid Membranes,” *Chinese J. Chem. Eng.*, vol. 17, no. 4, pp. 594–601, 2009, doi: 10.1016/S1004-9541(08)60249-9.

[28] T. He, “Towards stabilization of supported liquid membranes: preparation and characterization of polysulfone support and sulfonated poly (ether ether ketone) coated composite hollow fiber membranes,” *Desalination*, vol. 225, no. 1–3, pp. 82–94, 2008, doi: 10.1016/j.desal.2007.04.090.

[29] T. T. Van Tran, C. H. Nguyen, W. C. Lin, and R. S. Juang, “Improved stability of a supported liquid membrane process via hydrophobic modification of PVDF support by plasma activation and chemical vapor deposition,” *Sep. Purif. Technol.*, vol. 277, no. August, p. 119615, 2021, doi: 10.1016/j.seppur.2021.119615.

[30] Y. T. Ong, K. F. Yee, Y. K. Cheng, and S. H. Tan, “A review on the use and stability of supported liquid membranes in the pervaporation process,” *Sep. Purif. Rev.*, vol. 43, no. 1, pp. 62–88, 2014, doi: 10.1080/15422119.2012.716134.

[31] C. Das and K. A. Gebru, *Polymeric Membrane Synthesis, Modification, and Applications, Electro-Spun and Phase Inverted Membranes*. CRC Press, Taylor & Francis, 2019.

[32] Y. Alqaheem and A. A. Alomair, “Minimizing Solvent Toxicity in Preparation of Polymeric Membranes for Gas Separation,” *ACS Omega*, vol. 5, no. 12, pp. 6330–6335, 2020, doi: 10.1021/acsomega.9b03656.

[33] G. Van Eygen *et al.*, “Facilitated solvent screening for membrane-based extraction of chiral amines via a priori simulations,” *J. Mol. Liq.*, vol. 375, p. 121351, 2023, doi: 10.1016/j.molliq.2023.121351.

[34] P. Heikkilä and A. Harlin, “Parameter study of electrospinning of polyamide-6,” *Eur. Polym. J.*, vol. 44, pp. 3067–3079, 2008, doi: 10.1016/j.eurpolymj.2008.06.032.

[35] C. Mit-uppatham, M. Nithitanakul, and P. Supaphol, “Ultrafine Electrospun Polyamide-6 Fibers: Effect of Solution Conditions on Morphology and Average Fiber Diameter,” *Macromol. Chem. Phys.*, vol. 205, pp. 2327–2338, 2004, doi: 10.1002/macp.200400225.

[36] A. Azari, A. Golchin, M. M. Maymand, F. Mansouri, and A. Ardeshirylajimi, “Electrospun Polycaprolactone Nanofibers: Current Research and Applications in Biomedical Application,” *Adv. Pharm. Bull.*, vol. 12, no. 4, pp. 658–672, 2022, doi: 10.15171/jcvtr.2015.24.

[37] T. Meireman, L. Daelemans, S. Rijckaert, H. Rahier, W. Van Paepegem, and K. De Clerck, “Delamination resistant composites by interleaving bio-based long-chain polyamide nanofibers through optimal control of fiber diameter and fiber morphology,” *Compos. Sci. Technol.*, vol. 193, p. 108126, 2020, doi: 10.1016/j.compscitech.2020.108126.

[38] S. Lauren, “Surface free energy – what is it and how to measure it ?,” *Biolin Scientific*.

[39] W. Li, C. Molina-Fernández, J. Estager, J. C. M. Monbaliu, D. P. Debecker, and P. Luis, “Supported ionic liquid membranes for the separation of methanol/dimethyl carbonate mixtures by pervaporation,” *J. Memb. Sci.*, vol. 598, no. October 2019, pp. 1–10, 2020, doi: 10.1016/j.memsci.2019.117790.

[40] H. W. Khan, A. V. B. Reddy, M. M. E. Nasef, M. A. Bustam, M. Goto, and M. Moniruzzaman, “Screening of ionic liquids for the extraction of biologically active compounds using emulsion liquid membrane: COSMO-RS prediction and experiments,” *J. Mol. Liq.*, 2020, doi: 10.1016/j.molliq.2020.113122.

[41] Z. Zhang, R. Lu, Q. Zhang, J. Chen, and W. Li, “COSMO-RS based ionic liquid screening for the separation of acetonitrile and ethanol azeotropic mixture,” *J. Chem. Technol. Biotechnol.*, 2020, doi: 10.1002/jctb.6305.

[42] J. P. Wojeicchowski, C. Marques, L. Igarashi-Mafra, J. A. P. Coutinho, and M. R. Mafra, “Extraction of phenolic compounds from rosemary using choline chloride – based Deep Eutectic Solvents,” *Sep. Purif. Technol.*, 2021, doi: 10.1016/j.seppur.2020.117975.

[43] D. Xu, J. Chow, C. C. Weber, M. A. Packer, S. Baroutian, and K. Shahbaz, “Evaluation of deep eutectic solvents for the extraction of fucoxanthin from the alga Tisochrysis lutea - COSMO-RS screening and experimental validation,” *J. Environ. Chem. Eng.*, vol. 10, no. 5, p. 108370, 2022, doi: 10.1016/j.jece.2022.108370.

[44] F. Galiano, “Immersion casting,” in *Encyclopedia of Membranes*, 2015, pp. 1–2.

[45] A. K. Holda, B. Aernouts, W. Saeys, and I. F. J. Vankelecom, “Study of polymer concentration and evaporation time as phase inversion parameters for polysulfone-based SRNF membranes,” *J. Memb. Sci.*, vol. 442, pp. 196–205, 2013, doi: 10.1016/j.memsci.2013.04.017.

[46] D. E. Packham, “Surface energy , surface topography and adhesion,” *Int. J. Adhes. Adhes.*, vol. 23, no. 6, pp. 437–448, 2003, doi: 10.1016/S0143-7496(03)00068-X.

[47] K.-Y. Law and H. Zhao, “Determination of solid surface tension by contact angle,” in *Surface*

Wetting: characterization, contact angle, and fundamentals, 2016, pp. 135–148.

[48] A. Rudawska, *Surface treatment in bonding technology*. Academic Press, 2019.

[49] X. Hao, J. Zhang, Y. Guo, and H. Zhang, "Studies on Porous and Morphological Structures of Expanded PTFE Membrane through Biaxial Stretching Technique," *Int. Nonwovens J.*, vol. 14, no. 2, pp. 31–38, 2005, doi: 10.1177/1558925005os-1400205.

[50] P. Dzygieł, P. Wieczorek, and P. Kafarski, "Supported liquid membrane separation of amine and amino acid derivatives with chiral esters of phosphoric acids as carriers," *J. Sep. Sci.*, vol. 26, pp. 1050–1056, 2003, doi: 10.1002/jssc.200301445.